Octave-spanning ultrafast OPO with 2.6-6.1µm instantaneous bandwidth pumped by femtosecond Tm-fiber laser

Nick Leindecker,[1,*] Alireza Marandi,[1] Robert L. Byer,[1] Konstantin L. Vodopyanov,[1] Jie Jiang,[2] Ingmar Hartl,[2] Martin Fermann,[2] and Peter G. Schunemann[3]

[1]E.L. Ginzton Laboratory, Stanford University, Stanford California 94305, USA
[2]IMRA America Inc., 1044 Woodridge Ave. Ann Arbor Michigan 48105, USA
[3]BAE Systems, PO Box 868 Nashua New Hampshire 03063, USA
[*]nick.leindecker@stanford.edu

Abstract: We report the extension of broadband degenerate OPO operation further into mid-infrared. A femtosecond thulium fiber laser with output centered at 2050 nm synchronously pumps a 500-µm-long crystal of orientation patterned GaAs providing broadband gain centered at 4.1 µm. We observe a pump threshold of 17 mW and output bandwidth extending from 2.6 to 6.1 µm at the −30 dB level. Average output power was 37 mW. Appropriate resonator group dispersion is a key factor for achieving degenerate operation with instantaneously broad bandwidth. The output spectrum is very sensitive to absorption and dispersion introduced by molecular species inside the OPO cavity.

©2012 Optical Society of America

OCIS codes: (190.4975) Parametric processes; (190.4410) Nonlinear optics, parametric processes.

References and links

1. T. Popmintchev, M.-C. Chen, P. Arpin, M. M. Murnane, and H. C. Kapteyn, "The attosecond nonlinear optics of bright coherent X-ray generation," Nat. Photonics **4**(12), 822–832 (2010).
2. P. B. Corkum and F. Krausz, "Attosecond science," Nat. Phys. **3**(6), 381–387 (2007).
3. C. M. S. Sears, E. Colby, R. J. England, R. Ischebeck, C. McGuinness, J. Nelson, R. Noble, R. H. Siemann, J. Spencer, D. Walz, T. Plettner, and R. L. Byer, "Phase stable net acceleration of electrons from a two-stage optical accelerator," Phys. Rev. Lett. **11**, 101301 (2008).
4. M. J. Thorpe, D. Balslev-Clausen, M. S. Kirchner, and J. Ye, "Cavity-enhanced optical frequency comb spectroscopy: application to human breath analysis," Opt. Express **16**(4), 2387–2397 (2008).
5. S. A. Diddams, L. Hollberg, and V. Mbele, "Molecular fingerprinting with the resolved modes of a femtosecond laser frequency comb," Nature **445**(7128), 627–630 (2007).
6. F. Keilmann, C. Gohle, and R. Holzwarth, "Time-domain mid-infrared frequency-comb spectrometer," Opt. Lett. **29**(13), 1542–1544 (2004).
7. F. Adler, K. C. Cossel, M. J. Thorpe, I. Hartl, M. E. Fermann, and J. Ye, "Phase-stabilized, 1.5 W frequency comb at 2.8-4.8 microm," Opt. Lett. **34**(9), 1330–1332 (2009).
8. C. D. Nabors, S. T. Yang, T. Day, and R. L. Byer, "Coherence properties of a doubly-resonant monolithic optical parametric oscillator," J. Opt. Soc. Am. B **7**(5), 815–820 (1990).
9. S. T. Wong, T. Plettner, K. L. Vodopyanov, K. Urbanek, M. Digonnet, and R. L. Byer, "Self-phase-locked degenerate femtosecond optical parametric oscillator," Opt. Lett. **33**(16), 1896–1898 (2008).
10. S. T. Wong, K. L. Vodopyanov, and R. L. Byer, "Self-phase-locked divide-by-2 optical parametric oscillator as a broadband frequency comb source," J. Opt. Soc. Am. B **27**(5), 876–882 (2010).
11. N. Leindecker, A. Marandi, R. L. Byer, and K. L. Vodopyanov, "Broadband degenerate OPO for mid-infrared frequency comb generation," Opt. Express **19**(7), 6296–6302 (2011).
12. K. L. Vodopyanov, E. Sorokin, I. T. Sorokina, and P. G. Schunemann, "Mid-IR frequency comb source spanning 4.4-5.4 µm based on subharmonic GaAs optical parametric oscillator," Opt. Lett. **36**(12), 2275–2277 (2011).
13. J. Jiang, A. Ruehl, I. Hartl, and M. E. Fermann, "Tunable coherent Raman soliton generation with a Tm-fiber system," **CThBB5** CLEO 2011, Baltimore, Maryland, USA.
14. J. P. Gordon, "Theory of the soliton self-frequency shift," Opt. Lett. **11**(10), 662–664 (1986).
15. F. M. Mitschke and L. F. Mollenauer, "Discovery of the soliton self-frequency shift," Opt. Lett. **11**(10), 659–661 (1986).

---

16. C. B. Ebert, L. A. Eyres, M. M. Fejer, and J. S. Harris, Jr., "MBE growth of antiphase GaAs films using GaAs/Ge/GaAs heteroepitaxy," J. Cryst. Growth **202**, 187–193 (1999).
17. The HITRAN Database, http://www.cfa.harvard.edu/HITRAN/
18. V. L. Kalashnikov and E. Sorokin, "Soliton absorption spectroscopy," Phys. Rev. A **81**(3), 033840 (2010).
19. A. Foltynowicz, T. Ban, P. Masłowski, F. Adler, and J. Ye, "Quantum-noise-limited optical frequency comb spectroscopy," Phys. Rev. Lett. **107**(23), 233002 (2011).
20. J. Jiang, C. Mohr, J. Bethge, M. E. Fermann, and I. Hartl, "Fully stabilized, self-referenced thulium fiber frequency comb," CLEO Europe 2011, p. PDB-1.
21. J. Bethge, J. Jiang, C. Mohr, M. E. Fermann, and I. Hartl, "Optically referenced Tm-fiber-laser frequency comb," ASSP 2012, p. AT5A.3.

1. Introduction

A coherent source with broad instantaneous bandwidth and absolute frequency stability has many applications. Indeed, the advent of frequency combs and excellent mode-locked fiber lasers have revolutionized precision metrology in the visible and near-infrared. The extension of comb sources to the mid-infrared enables exciting applications such as X-ray production via high harmonic generation [1], attosecond physics [2], laser-driven particle acceleration [3], trace gas detection [4], and molecular fingerprinting [5] but remains technically challenging [6, 7]. A degenerate OPO is in principle a nearly ideal frequency converter [8, 9], capable of extending the benefits of frequency combs to the mid-IR through rigorous, phase and frequency locked down conversion of established mode-locked pump lasers. With the high peak intensity of the pump source and the inherent double resonance of the degenerate OPO, this conversion is accomplished with low threshold and high efficiency. We extend our earlier work [10–12] by pumping at 2-µm with a Tm-fiber laser and by employing GaAs as a nonlinear element, again achieving extremely broad bandwidth output, but now spanning an octave in the spectroscopically important 'fingerprint' band.

2. Methods

A schematic overview of our OPO system is presented in Fig. 1. The pump is a thulium fiber oscillator-amplifier system operating at 2050nm. The oscillator is based on a linear cavity soliton fiber laser incorporating a chirped fiber Bragg grating for dispersion compensation. It is mode-locked by a saturable absorber mirror, ensuring self-starting operation at a repetition frequency of 75 MHz [13]. The oscillator was pumped by a low relative intensity noise (RIN) semiconductor laser at 1564nm, which was amplified in an Er-fiber amplifier chain to an average power of 1.3W. The 300 fs pulses from the oscillator have an average power of 10 mW and a center wavelength of 1950 nm. They are amplified and compressed in a cladding pumped Tm-fiber amplifier. The amplifier is operated in a slightly nonlinear regime, where nonlinearities including Raman-self soliton shift [14, 15] in the anomalous dispersive Tm-doped amplifier fiber lead to both spectral broadening (to 60 nm) and a red-shift of the pulse center wavelength to 2050nm. With a pump power of 25W at 793nm, the laser systems output produces soliton pulses at a pulse-duration of 93 fs with up to 1 W average power.

The OPO resonator is a 4 m long ring cavity that is matched in length to the pump repetition rate of 75 MHz. The intracavity optics comprise a flat dielectric mirror M_1 with high transmission (>95%) for the pump and high reflectivity in the 3–6 µm range, and 5 gold coated mirrors $M_2 - M_6$ with high (99%) mid-IR reflection. Mirrors M_2 and M_3 are concave with the radius of curvature $R = 50$ mm, and mirrors $M_4 - M_6$ are flat.

Broadband gain centered at 4.1 µm is provided by a short, $L = 0.5$-mm, quasi-phase-matched (QPM) orientation-patterned gallium arsenide (OP-GaAs) crystal. The OP-GaAs structure was grown at BAE Systems by a combination of molecular beam epitaxy and hydride vapor phase epitaxy [16], resulting in QPM "film" thickness of >1 mm. The samples have a usable aperture of 1 × 4 mm. The QPM period is 60.5 µm, suitable for room-temperature subharmonic generation from the 2 µm pump and amounts to only 8 domain reversal periods. The crystal was cut and polished for Brewster-angled application such that, after entering the crystal at Brewster angle, all interacting beams propagate along <011>

direction, perpendicular to the inverted domain boundaries, and polarizations of all interacting waves are parallel to <111 > direction in GaAs.

An 80 μm-thick plane-parallel plate of YAG with group velocity dispersion (GVD, $d^2k/d\omega^2$) of −1190 fs^2/mm at 4.1 µm is inserted inside the cavity at near Brewster angle to partly compensate the positive GVD of GaAs (390 fs^2/mm at 4.1 µm). Output is taken as Fresnel reflection from the plate or simply leaked through the dielectric mirror M1.
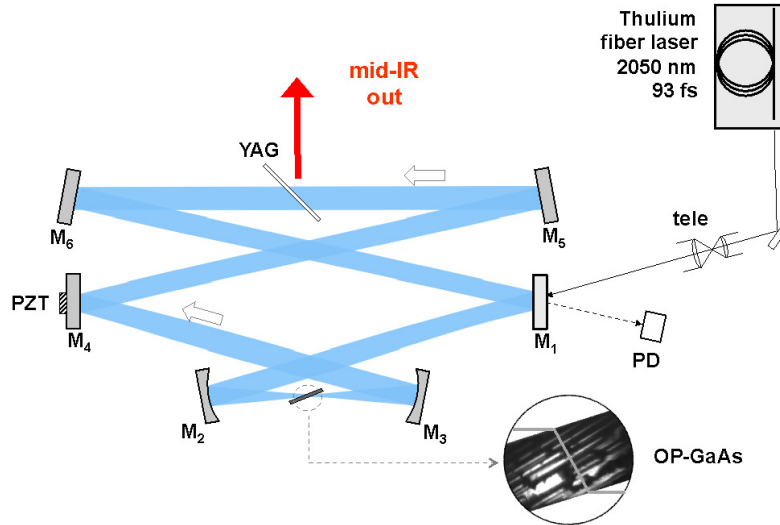
Fig. 1. Schematic of the ring-cavity OPO setup. M1 is a dielectric mirror for in-coupling the pump, M2 and M3 are concave and M4-M6 is flat gold-coated mirrors, PZT - piezo actuator stage. A thin YAG plate provides partial second-order GVD compensation. The photodetector PD consists of a photoconductive PbSe element behind a long pass (> 2.5 µm) filter.

With this ring OPO cavity configuration, the eigenmode beam waist size ($1/e^2$ intensity radius) inside the GaAs crystal at 4.1 μm was calculated to be w = 14.5 µm. The pump laser beam is conditioned by a telescope (Fig. 1) to a diameter and wave front curvature before mirror M1 such that after reflecting from curved mirror M2 its waist was inside the GaAs crystal with the beam size of approximately w = 10 µm, close to a confocal pumping condition. Astigmatism inside the OPO cavity, caused by the Brewster-angled GaAs is compensated by the opposite-sign astigmatism due to oblique (3°) incidence on the curved mirrors.
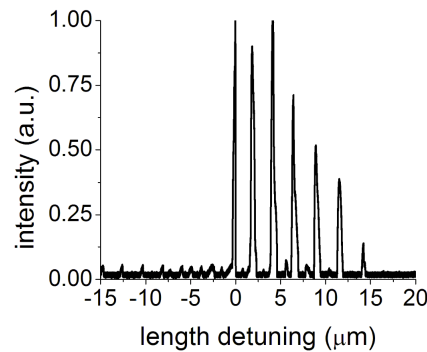

Fig. 2. OPO output intensity as a function of roundtrip cavity length consists of a number of discrete oscillation peaks separated by approximately the pump center wavelength. The small interleaved peaks and those extending to shorter length detunings are associated with the secondary set of longitudinal modes due to extra dispersion caused by intracavity carbon dioxide.

3. Results

Oscillation occurs when the OPO signal/idler waves are brought into simultaneous resonance near degeneracy by fine-tuning the cavity length with the piezo stage (PZT) attached to M_4. Since double resonance occurs at only discrete set of lengths, we observe oscillation 'peaks' when the cavity length is scanned (Fig. 2). Continuous operation of the OPO may be obtained by locking the cavity length to track one of these resonances.

When operated with minimum roundtrip loss, estimated to be 15%, we observe an OPO threshold of 17 mW for a 0.5-mm GaAs crystal. As pump power is increased, oscillation occurs at additional discrete length detunings satisfying the doubly-resonant OPO condition. At full pump power, we observe oscillation at over 20 discrete lengths. With the 610 mW of pump power, and an outcoupling of 4%, we extracted 37 mW of average power in the mid-IR. We have not attempted to optimize the outcoupling.

Spectra of the OPO output were measured with (i) high, 0.5 cm^{-1}, spectral resolution using an FTIR spectrometer equipped with a photovoltaic MCT (mercury cadmium telluride, 1-12 µm) detector cooled to 77K and (ii) low resolution, 5 cm^{-1}, but higher dynamic range using a f = 20cm monochromator equipped with a 100 line/mm diffraction grating. For greater convenience, a thermoelectrically cooled photoconductive InSb detector (1-6.1 µm) was occasionally substituted for the MCT detector when using the monochromator. A long pass (> 2.5 µm) filter on germanium substrate was used to reject residual 2050-nm pump.

The 2D color intensity plots of Fig. 3 represent the output spectra (taken through mirror M1) obtained with the monochromator for different cavity length detunings. In this case, for each monochromator position, the cavity length was continuously varied and monochromator detector signal recorded. Each horizontal 'stripe' corresponds to one of the resonant peaks in the OPO output. In Fig. 3(a), the OPO runs un-purged with the dispersion of the 0.5-mm GaAs crystal un-compensated. In (b), 80-um YAG is added to partially compensate GaAs dispersion. In (c), the OPO is purged with dry nitrogen but has no YAG compensation. In (d), 80-µm YAG is added to the purged OPO. As expected, the shapes of the output spectra are found to depend significantly on which of the discrete resonant cavity-length peaks the OPO is tuned.
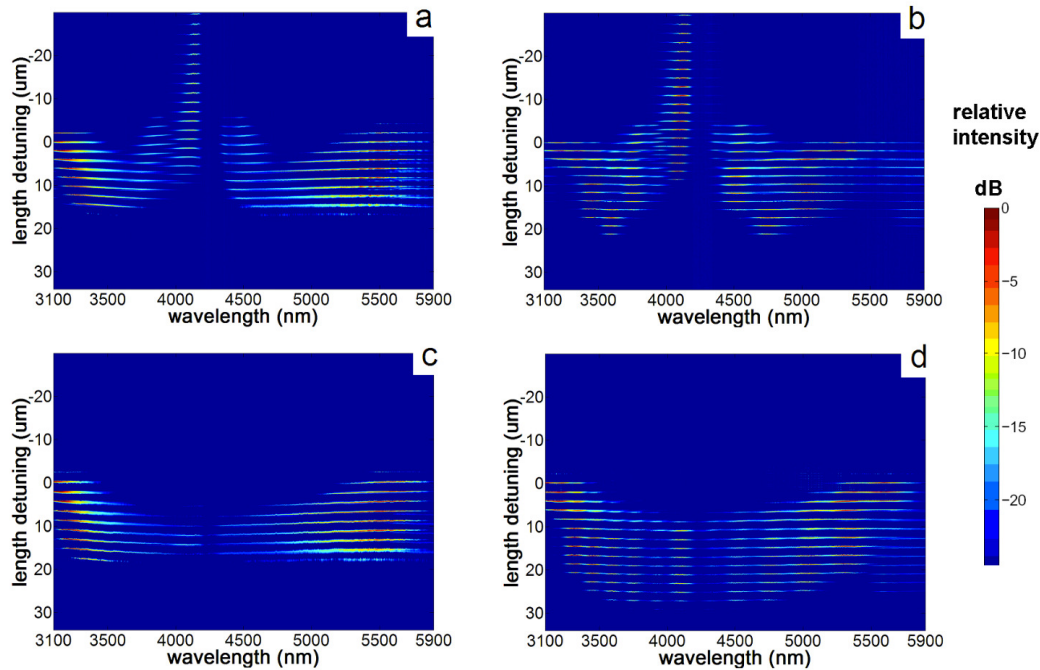
Fig. 3. 2D color intensity plots of the output spectra as the resonator length is detuned. In (a), the OPO runs un-purged with the dispersion of the 0.5-mm GaAs crystal un-compensated. In (b), 80-um YAG is added to partially compensate GaAs dispersion. In (c), the OPO is purged with dry nitrogen but has no YAG compensation. In (d), 80-μm YAG is added to the purged OPO.

In the case of unpurged cavity, Fig. 3(a,b), the presence of atmospheric carbon dioxide dramatically changes the shape of the 2D plot due to the extra group velocity dispersion and absorption (in the vicinity of 4.25 μm) introduced inside the cavity. Un-purged, the OPO operates toward shorter de-tuned lengths, albeit with a narrow spectrum centered near 4.1 μm (the result of extra group dispersion due to CO_2 in the atmosphere), while the output in the center of the band (4.25 μm) is completely suppressed. When the resonator is purged, the effects of CO_2-related intracavity dispersion and absorption are mostly removed, and the spectrum vs. length plots take on a much simpler character. Broad instantaneous bandwidth is achieved with appropriate dispersion compensation and the OPO locked to a suitable peak.

Figure 4 shows representative OPO output spectra when the OPO cavity length is electronically locked to one of the cavity resonances using a piezo actuator stage and a technique similar to [11]. Figure 4(a) shows both degenerate (gray) and non-degenerate (black) operation. In the former case, 'gap-less' degenerate operation was achieved over a narrower overall bandwidth at an intermediate stage in the purge process, while the non-degenerate spectrum was recorded prior to purging. Figure 4(b) shows the broadest output spectrum achieved without purging and Fig. 4(c) - the broadest spectrum achieved with the resonator purged. In all cases, a YAG plate was used for dispersion compensation. The spectra of Fig. 4(b,c) correspond to the broadest bandwidth we have measured, which extends from 2.6 to 6.1 μm at a level 30 dB below the peak value, albeit with a small gap believed to be associated with residual carbon dioxide. All output spectra exhibit some dip at 4.2-4.3 μm due to absorption by atmospheric CO_2 (even in the 'purged' case, there is residual CO_2 in the resonator, and a ~2 m unpurged path to the detector). We estimate the spectral density of the output to be 100 nW per comb line.
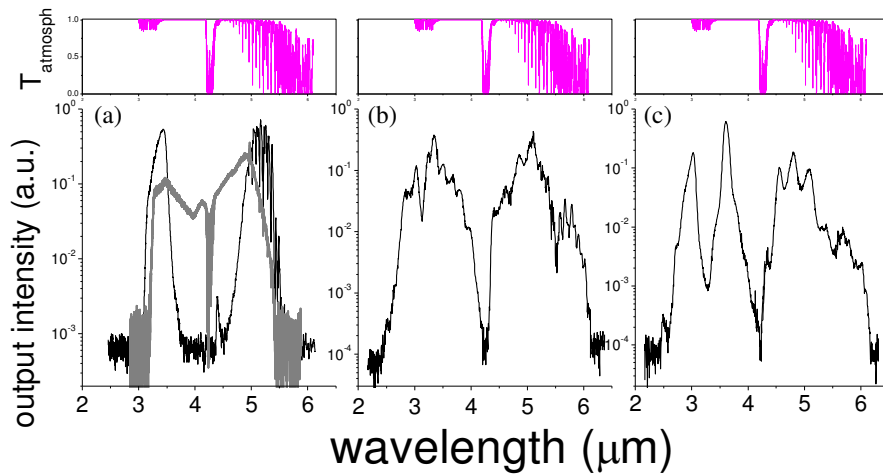
Fig. 4. Representative OPO output spectra with YAG plate used for dispersion compensation. (a) Degenerate (gray) and non-degenerate (black) output. In the former case, the 'gap-less' degenerate operation was achieved over a narrower overall bandwidth at an intermediate stage in the purge process, while the non-degenerate spectrum was recorded prior to purging. (b) The broadest output spectrum that was achieved without purging. (c) The broadest spectrum achieved with the resonator purged. The dips in the spectra around 4.25 μm are all due to absorption of atmospheric carbon dioxide; transmission through 2 m of atmosphere is shown on top.

When the cavity is not purged, we observe strong modulation of the output spectrum due to water-vapor lines, carbon dioxide and also isotopic ($^{13}CO_2$) carbon dioxide (Fig. 5). The spectral features we observe correlate well with the HITRAN database [17], however on some occasions they show 'dispersive' features and look like a superposition of absorption dips and their first derivatives, with the 'gain' observed on the low-frequency side of the peaks (which is especially pronounced for the water-vapor lines). Similar intracavity effects near molecular resonances have previously been observed with a femtosecond mid-IR Cr:ZnSe laser [18], femtosecond Cr:ZnSe laser pumped OPO [12], and with a near-IR frequency comb spectrometer which uses an external high-finesse enhancement cavity [19]. We believe that, similar to the model of [19], the dispersive shape of absorption lines is caused by the fact that far from the OPO degeneracy point, dispersion of the cavity causes a mismatch between the cavity modes and the comb of modes dictated by the pump laser. Near molecular resonances, dispersion may shift the cavity modes closer to the comb line centers, causing local intensity overshoot in the absorption line shapes.
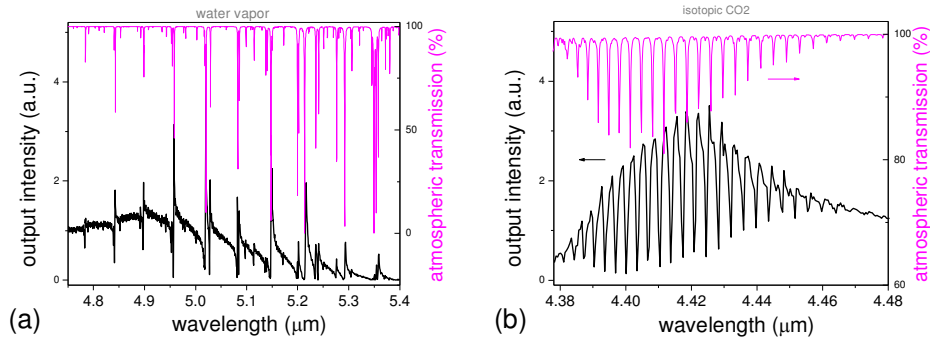
Fig. 5. Modulation of the OPO spectrum near λ = 5 μm associated with intracavity water vapor absorption (left) and near 4.4 μm due to isotopic carbon dioxide ($^{13}CO_2$) (right) in an un-purged cavity measured with a FTIR spectrometer. Percent transmission through 4 m of standard atmosphere (from HITRAN database) is shown in magenta.

Our calculations suggest that the OPO spectral bandwidth is limited by (i) mirror coatings, (ii) bandwidth of parametric gain, and (iii) intracavity group delay dispersion. Figure 6(a) shows wavelength dependence of the reflectivity of the dielectric mirror (M1 of Fig. 1) and also relative parametric gain of the 0.5-mm OP-GaAs crystal. Figure 6(b) shows cumulative relative group delay per roundtrip introduced by 0.5-mm GaAs plus 80-μm YAG plus dielectric mirror (solid curve) and group delay without YAG plate (dashed curve). We assumed that dispersion of air and metallic mirrors is negligible. Although the group delay dependence becomes much flatter when dispersion compensating 80-μm YAG is added, the 3-rd order GVD remains uncompensated. With the ability to use shorter GaAs crystals (with larger gain bandwidth and less intrinsic dispersion), and chirped dielectric mirrors for dispersion compensation, we expect to achieve more uniform spectrum and access even greater bandwidth.
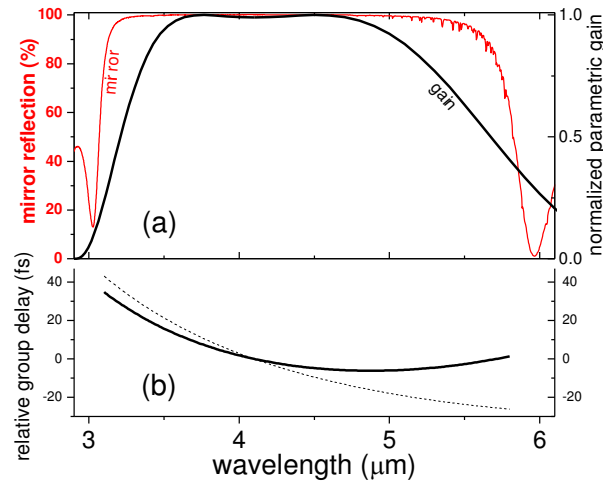

Fig. 6. (a) Reflectivity curve of the dielectric mirror (red curve) and relative parametric gain of the 0.5-mm OP-GaAs (black curve) vs. wavelength. (b) Cumulative group delay introduced by 0.5-mm GaAs plus 80-μm YAG plus dielectric mirror (solid curve) and group delay without YAG plate (dashed curve).

4. Conclusion

We have shown that a degenerate GaAs-based OPO pumped by a Tm-fiber laser offers an extremely broad bandwidth output of over an octave from 2.6 to 6.1 µm – a range where OH, CH, CO, and NH chemical bonds show their strongest vibrational signatures. Proper intracavity dispersion management is essential for achieving such wide bandwidths.

In addition to the broad frequency coverage, the low pulse energy required to reach OPO threshold and the predicted phase locking of the signal/idler to the pump render this system a potentially ideal source for precision frequency comb spectroscopy in the mid IR.

Note added in proof: Preliminary results with an OPO of similar design, pumped by a stabilized Tm fiber frequency comb laser [20, 21], confirm that the OPO runs fully carrier phase locked with sub 300 kHz comb line width.

Acknowledgments